Electrode/Electrolyte Interface in Sulfolane-Based Electrolytes for Li Ion Batteries: A Molecular Dynamics Simulation Study

ARTICLE *in* THE JOURNAL OF PHYSICAL CHEMISTRY C · OCTOBER 2012

Impact Factor: 4.77 · DOI: 10.1021/jp3054179

THE JOURNAL OF PHYSICAL CHEMISTRY C

Article

pubs.acs.org/JPCC

Electrode/Electrolyte Interface in Sulfolane-Based Electrolytes for Li Ion Batteries: A Molecular Dynamics Simulation Study

Lidan Xing,[†,‡] Jenel Vatamanu,*[,†] Oleg Borodin,[§] Grant D. Smith,[∥] and Dmitry Bedrov[†]

[†]Department of Materials Science and Engineering, University of Utah, 122 S. Central Campus Dr., Salt Lake City, Utah 84112, United States

[‡]School of Chemistry and Environment, South China Normal University, Guangzhou 510006, China

[§]Electrochemistry Branch, Army Research Laboratory, 2800 Powder Mill Rd., Adelphi, Maryland 20783, United States

[∥]Wasatch Molecular Inc., Salt Lake City, Utah 84103, United States

ABSTRACT: The double layer composition and structure of the mixed-solvent electrolyte tetramethylene sulfone/dimethyl carbonate (TMS/DMC) doped with $LiPF_6$ near the graphite surface have been investigated using molecular dynamics simulations as a function of applied potential between the electrodes ranging from 0 to 6 V. Three solvent compositions, with TMS/DMC ratios of 1:2, 1:1, and 2:1 doped with $LiPF_6$ salt, were investigated. At uncharged electrodes, electrolyte composition at the interfaces was found to be similar to that of bulk electrolyte for TMS/DMC ratios of 1:1 and 1:2 systems but deviated from the bulk for a TMS/DMC ratio of 2:1. At negative electrodes the polar solvent TMS preferentially adsorbs at the electrode surface displacing the almost nonpolar DMC solvent. The preferential partitioning of TMS relative to DMC to the negative electrode surface is consistent with the stronger binding of the former with Li^+ that partitions to the anode surface as potential becomes more negative as well as with the ability of relatively polar TMS to better respond to the electrostatic potential near a charged surface. At the positive electrode, TMS/DMC ratios were found to be similar to bulk compositions that is different to the behavior observed in ethylene carbonate (EC)/DMC/$LiPF_6$ electrolyte where preferential partitioning of a more polar EC molecule was observed on both electrodes. Our results also show that, in TMS/DMC/$LiPF_6$ electrolyte, DMC is located approximately 0.8 Å further way from the positive electrode than in EC/DMC/$LiPF_6$ indicating that it might be more difficult to oxidize DMC in the TMS-based electrolytes that is consistent with experimentally reported increased oxidative stability of the latter. Finally, changes of the Li^+ solvation shell and double layer capacitance were analyzed as a function of electrode potential.

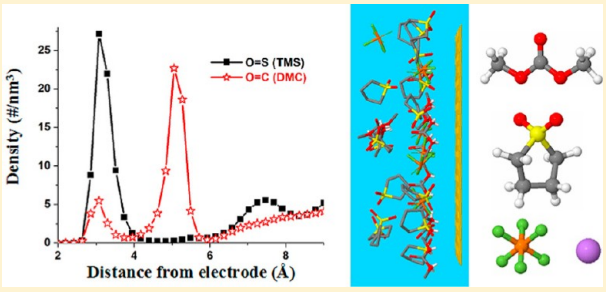

1. INTRODUCTION

Development of high energy, density high voltage batteries and electrical double layer (EDL) capacitors requires electrolytes with high electrochemical stability windows.[1,2] A number of solvents or additives have been recently considered as agents to improve electrochemical stability of electrolytes in these applications.[3] Tetramethylene sulfone (TMS or sulfolane)-based electrolytes were shown to have high oxidative stability[4,5] and good cycling ability in a cell with high voltage $LiNi_{0.5}Mn_{1.5}O_4$ spinel cathodes.[6] However, the high viscosity of sulfone-based electrolytes such as TMS or ethyl methyl sulfone (EMS) doped with $LiPF_6$ or LiTFSI salts limits the battery charge and discharge rates. Addition of low viscosity thinning solvents such as ethyl methyl carbonate (EMC) increases conductivity, wetting of the electrode and separator surfaces.[7] TMS/DMC/LiTFSI electrolytes have been shown to retain sufficient oxidative stability and allow 1000 cycles against high voltage $LiNi_{0.5}Mn_{1.5}O_4$ spinel at 2C rates.[6] Interestingly, a mixture of ethyl acetate, a solvent with low oxidative stability, and a high oxidative stability TMS solvent doped with Bu_4NBF_4 on Pt showed oxidative stability much higher than the ethyl acetate based electrolyte and only slightly worse than the pure TMS-based electrolyte.[8] These results suggest that the oxidative stability of TMS-based electrolytes mixed with linear carbonate or acetate solvents is not determined by the component with the lowest oxidative stability (carbonate or acetate) and may be in fact similar to that of TMS electrolytes without low viscosity additives.

We believe the redox stability of electrolyte/additive mixtures can be related, at least in part, to the double layer structure of electrolyte at electrode surfaces where the redox processes take place. For example, molecular dynamics (MD) simulations of bulk EC/dimethyl carbonate (DMC)(1:1)/$LiPF_6$ electrolytes showed equal coordination of Li^+ by EC and DMC molecules.[9] Hence, if Li^+ approaching the anode surface has retained its bulk coordination, one could expect an equal amount of EC and DMC decomposition products in the solid/electrolyte interphase (SEI) formation on the negative electrode. However,

Received: June 2, 2012
Revised: September 21, 2012
Published: September 25, 2012

   dx.doi.org/10.1021/jp3054179 | J. Phys. Chem. C 2012, 116, 23871−23881

most experimental works conclude that initial stages of SEI formation are dominated by decomposition products of EC.[7] Our recent simulation studies of EC/DMC(1:2.25)/$LiPF_6$ electrolyte[10] demonstrated that the highly polar EC preferentially adsorbs at the electrode surfaces displacing relatively nonpolar DMC solvent as the electrodes are charged. Therefore, the changes of electrolyte interfacial layer composition predicted by molecular simulations as a function of electrode potential allowed us to provide the molecular level rationale to experimental observations for this electrolyte reduction decomposition. Solvent molecules that preferentially adsorb to the electrode surface or coordinate the intercalated Li^+ are expected to have a preference to undergo redox reactions, and therefore, it is important to understand the composition and the structure of the interfacial layer as functions of electrode potential. Moreover, the composition and structure of the double layer were shown to influence the free energy for the Li^+ desolvation that is closely related to the interfacial resistance for Li^+ intercalation.[10,11]

In this manuscript, we report a simulation study of the double layer composition and structural properties for TMS/DMC mixed-solvent electrolytes doped with $LiPF_6$ that were sandwiched between graphite electrodes as a function of applied potential. We have investigated three solvent compositions with TMS/DMC molar ratios of 1:2, 1:1, and 2:1 and have conducted a detailed analysis of the local electrolyte composition and the Li^+ solvation shell composition in the bulk and at electrode surfaces. The choice of DMC cosolvent and $LiPF_6$ salt facilitates systematic comparison between electrolytes studied here and an EC-based electrolyte (EC/DMC(1:2.25)/$LiPF_6$) studied earlier.[10] In this work, we chose to focus on graphite electrodes that also serve as model systems for EDL capacitors and carbon additives in lithium ion batteries.

2. SIMULATION METHODOLOGY

MD simulations were performed on mixed-solvent TMS/DMC electrolytes doped with $LiPF_6$ salt. Figure 1a shows the chemical structures of all compounds used to compose investigated electrolytes. All electrolytes contained 36 $LiPF_6$ salt pairs dissolved in 360 solvent molecules of TMS/DMC mixture, that is, a salt/solvent ratio of 1:10. Three solvent compositions with TMS/DMC molar ratios of 1:2, 1:1, and 2:1 were investigated as indicated in Table 1. The results obtained for these electrolytes were compared with our previous work[10] on $LiPF_6$ salt in the EC/DMC mixture with a EC/DMC ratio of 1:2.25 and a $LiPF_6$/solvent ratio of 1:12.

The simulation setup consisted of electrolyte confined between two graphite electrodes as illustrated in Figure 1b. The asymmetry direction, defined as the axis perpendicular to electrode surfaces, will be referred as the z axis. Each electrode was represented by two layers of graphite with the basal face exposed toward the electrolyte. In order to simplify our analysis, positions of graphite atoms were fixed during simulations. The cross-sectional area of the system was 25.614 Å × 24.647 Å, and the distance between electrodes varied between 94 and 96.5 Å, depending on the system composition. We verified that this separation between electrodes was sufficient to generate about a 30−35 Å wide layer of bulk-like electrolyte in the middle of the simulation cell.

The EC−$LiPF_6$ force field parameters were taken from ref 12 while the force field for TMS−$LiPF_6$ was parametrized to describe molecular mechanics calculations of binding energies

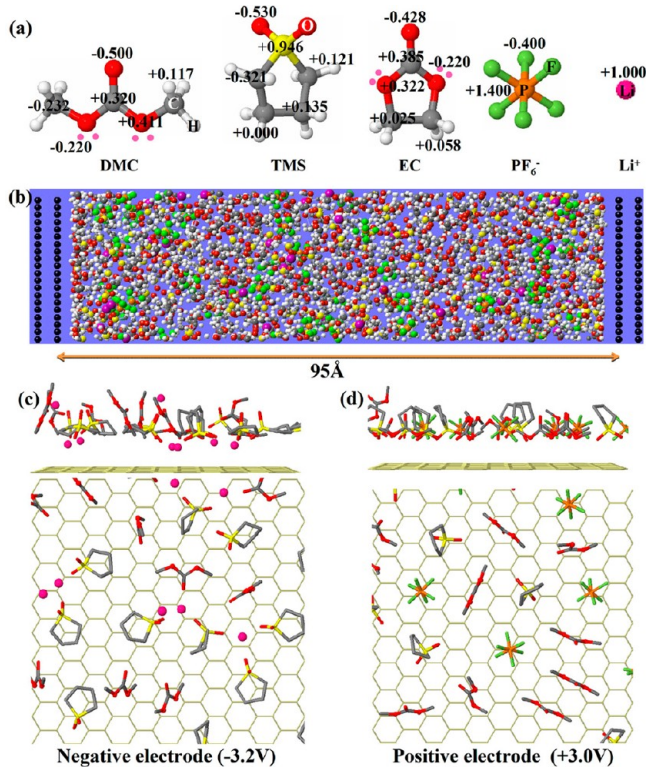

Figure 1. (a) Chemical structures and partial atomic charges of compounds studied in this work. In DMC and EC, small pink circles are the lone pairs attached to the ether oxygen atoms. (b) A snapshot of the simulation setup. (c, d) Snapshots of interfacial layers in electrolyte with a TMS/DMC ratio of 1:2 on negative and positive electrodes, respectively.

Table 1. Number of Molecules of Each Species in Investigated Systems

system	TMS or EC	DMC	$LiPF_6$
TMS/DMC (1:2)	120	240	36
TMS/DMC (1:1)	180	180	36
TMS/DMC (2:1)	240	120	36
EC/DMC	114	256	31

of $Li^+(TMS)_n(DMC)_m$ clusters with $n + m = 4$. The developed force field predicted that the stability of the cluster increases upon replacing DMC with TMS, with TMS_4/Li^+ being the most stable cluster and DMC_4/Li^+ being the least stable, which is in agreement with quantum chemistry (QC) calculations. Conductivity of TMS/DMC/$LiPF_6$ electrolytes predicted from MD simulations using this force field was also found in a good agreement with experiment. The electrode−electrolyte repulsion−dispersion cross-terms were calculated using the standard combining rules.[12] The polarizability of the electrolyte was represented with induced point dipoles placed on each atom. The short-range dipole−dipole interactions were damped utilizing the Thole[13] procedure.

The electrodes were treated as electronic conductors with the potential difference between two electrodes constrained to a desired value, utilizing constant potential methodology described elsewhere[14−16] and slightly modified for simulations with polarizable force fields.[10] In this approach, the potential difference between electrodes (not the charge on individual electrodes) is constrained during simulations. This provides more realistic conditions compared to simulations where

dx.doi.org/10.1021/jp3054179 | J. Phys. Chem. C 2012, 116, 23871−23881

homogeneously distributed charge is fixed on the electrode. In our simulations, as well as in real materials, the potential to the electrode is applied, and the charge on the electrode is determined by local electrostatic potential that in turn depends on the self-consistent interplay of several factors (e.g., heterogeneity of electrode structure, polarization due to restructuring of electrolyte at interface, etc.). When the system reaches stationary conditions, the total electrode charge fluctuates around an average value. The charge on the positive electrode is equal in magnitude and opposite in sign to the charge on the negative electrode and to the charge accumulated in the EDL formed next to the electrode due to excess build up of counterions.

The polarizability of the electrode is modeled via flexible Gaussian distributed charges with a width of 0.5 Å. The induced dipoles in electrolyte and the electrode charges are obtained by minimization of the electrostatic energy of the system with respect to each component of the induced dipole and each electrode charge.[10] The total electrostatic energy of the systems can be formally written as follows:

$$U = U_C + U_{self} + \frac{1}{2}\sum_{i=1}^{N\,dipoles}\frac{\boldsymbol{\mu}_i\boldsymbol{\mu}_i}{\alpha_i} - \sum_{i}^{electrode} V_i q_i \tag{1}$$

where U_C is the electrostatic energy due to interactions between all components (charges, dipoles), U_{self} is the energy due to self-interaction of Gaussian charges (not included in the U_C term), the α_i is the ion polarizability, and the last term is the work required to create charges q_i on the electrode atoms under condition of applied potential V_i for each electrode atom. The term U_C is given by the following relation:

$$U_C = \frac{1}{2}\sum_{\mathbf{k}^*}\sum_{i,j}\mathbf{Q}_i\mathbf{Q}_j\frac{1}{|\mathbf{R}_{ij}+\mathbf{kL}|} - \frac{1}{2}\sum_{\mathbf{k}^*}\sum_{i,j}\mathbf{Q}_i\mathbf{Q}_j\frac{1}{|\mathbf{R}_{ij}+\mathbf{kL}|}\mathrm{erfc}(\varepsilon_{ij}|\mathbf{R}_{ij}+\mathbf{kL}|) \tag{2}$$

where $\mathbf{Q}_i$ is a generalized charge defined as

$$\mathbf{Q}_i = q_i + \boldsymbol{\mu}_i \circ \nabla_i \tag{3}$$

where q is the electrostatic scalar charge and $\boldsymbol{\mu}_i$ is the induced dipole on atom i. All induced dipoles are placed on electrolyte atoms and are point distributed. The Gaussian cross-widths ε_{ij} are defined as follows:

$$\frac{1}{\varepsilon_{ij}^2} = \frac{1}{\varepsilon_i^2} + \frac{1}{\varepsilon_j^2} \tag{4}$$

where ε_i and ε_j are the widths of the individual Gaussian distributed charges i and j. Note that, for the electrolyte, atomic partial charges are represented as point charges, and therefore, for interaction within electrolyte, the second term of eq 2 becomes zero. $\mathbf{L}$ is the vector defining dimensions of the simulation cell, while vector $\mathbf{k}$ defines indices of periodic images of the simulation cell in the space filling construction. The $\mathbf{R}_{ij}$ is the distance vector between two charges i and j in the primary simulation cell ($\mathbf{k} = 0$), and the $\mathbf{kL}$ is distance offset between the charge i in the primary cell and the $\mathbf{k}$-th periodic image of charge j. The asterisk (*) in the summation over $\mathbf{k}$ indicates that the sum over charge pairs ij is constrained as $i \neq j$ when $k = 0$. The summation over $\mathbf{k}$ is done in the two-dimensional (2D) geometry, that is, in the x and y directions that are parallel to the electrode surfaces.

Taking into account that only the electrode atoms are represented as Gaussian distributed charges and have no induced dipoles, the self-interaction energy of Gaussian charges (the second term in eq 1) can be expressed as follows:

$$U_{self} = \sum_{i}^{electrode}\frac{q_i^2}{\sqrt{\pi}}\varepsilon_{ii} \tag{5}$$

where the summation is done only over all electrode atoms.

The electrode charges and the induced dipoles of the electrolyte were computed by solving simultaneously:

$$\frac{\partial U}{\partial q_{\mathbf{k}}^{electrode}} = 0, \qquad \frac{\partial U}{\partial \boldsymbol{\mu}_I^{electrolyte}} = 0 \tag{6}$$

In computing the energy in eq 1 and solving the system of eqs 6, the Smooth Particle Mesh Ewald (SPME) method adapted for 2D geometry[17] was utilized.

The MD simulations were conducted in the NVT ensemble at 333 K, and simulation cell dimensions adjusted such that the density of the electrolyte in the middle of the cell was equal to that of the bulk electrolyte at the corresponding temperature and atmospheric pressure. The latter was determined from bulk simulations in the NPT ensemble at the same thermodynamic conditions. The temperature was controlled using the Nose–Hoover thermostat.[18] Note that, due to ion accumulation near electrode surfaces, at high potentials (near ±3 V electrode potential), systems were slightly depleted of Li and PF_6 ions in the bulk region, that is, they had roughly 15% less ions in the bulk compared to systems with uncharged (or weakly charged) electrodes. Equations of motions were integrated using the RESPA method[19] with a 0.5 fs time step for the integration of forces from bonds, bends, and out-of-plane deformations, a 2.5 fs time step for forces from dihedrals and forces due to nonbonded interactions (van der Waals and the real part of electrostatic interactions) within a cutoff radius of 7.5 Å, and a 5 fs time step for the integration of the remaining nonbonded forces (i.e., van der Waals and electrostatic interactions within a 10.0 Å cut off and reciprocal part of SPME). Induced dipoles were computed every 5 fs while electrode charges were updated every 250 fs. Since positions of our electrode atoms are constrained, there are no intraelectrode relaxation/motion that can influence the local electric field. Hence, the local electric field on the electrode atoms only changes due to induction of image charges from electrolyte and is coupled to time scales of ionic/molecular rearrangement of the electrolyte at the surface. Empirically, we found that updating the electric field every time step is too conservative, since atomic positions of the electrolyte change very little within one integration time step. We verified that simulations with frequent (every time step) and less frequent updates of charges provided essentially identical results for all averaged properties studied, for the systems in equilibrium. Note, however, that, if dynamical relaxations of EDL structure during charging or discharging are of interest, then more frequent updates of electrode charges are needed, since the EDL structure is changing during these processes. In our simulations, each system was equilibrated for at least 4 ns followed by 60 ns production runs for each potential difference investigated.

Finally, while within our methodology the potential difference between two electrodes is constrained, the potentials on each electrode relative to the bulk electrolyte are not symmetric, that is, are not equal to one-half of the total

dx.doi.org/10.1021/jp3054179 | J. Phys. Chem. C 2012, 116, 23871–23881

applied potential with opposite signs. To determine the potential on each electrode relative to the bulk electrolyte, the Poisson potential across the simulation cell, $\phi(z)$, was computed by integrating the one-dimensional (1D) Poisson equation (i.e., transversely averaged):

$$\nabla_z[\varepsilon_0(\nabla_z\varphi(z))] - \nabla_z\boldsymbol{\mu}_z(z) = -\rho(z) \quad (7)$$

where ε_0 is the vacuum permittivity, $\rho(z)$ and $\boldsymbol{\mu}_z(z)$ are profiles of charge density and the z component of induced dipoles obtained from simulation, and ∇_z indicates the partial derivative along the z direction. The electric double layer potential (U_{EDL}) is defined as the difference between the Poisson potential on the electrode surface $\phi_{electrode}$ and the potential in the bulk electrolyte, ϕ_{bulk}, that is, in the middle of the simulation cell:

$$U_{EDL} = \varphi_{electrode} - \varphi_{bulk} \quad (8)$$

The potential of zero charge (PZC) is defined as the potential drop within the EDL near uncharged surfaces. All electrode potentials reported here are defined as EDL potential relative to PZC:

$$U_{electrode} = U_{EDL} - PZC = \varphi_{electrode} - \varphi_{bulk} - PZC \quad (9)$$

3. RESULTS AND DISCUSSION

3.1. Bulk Coordination of Li^+. First, we briefly summarize key results for the Li^+ solvation shell in the gas phase and bulk electrolytes. Molecular mechanics optimization of $Li^+(TMS)_n(DMC)_m$ clusters for $n + m = 4$ using the developed force field and ab initio calculations indicated that the substitution of TMS by DMC is energetically unfavorable. This is in contrast to similar investigation of $Li^+(EC)_n(DMC)_m$ clusters that showed that the lowest energy cluster consists of three EC and one DMC molecules.[15] Note that both EC and TMS molecules have a large dipole moment while DMC is almost nonpolar. In $Li^+(EC)_n(DMC)_m$ clusters, the alignment of only polar molecules around Li^+ is not always favorable, and therefore, inclusion of nonpolar molecules (such as DMC) in the first coordination shell allows other polar molecules to optimize their mutual orientations near Li^+ and can result in lower energy configurations of the cluster. However, our study of $Li^+(TMS)_n(DMC)_m$ clusters showed that the lowest energy configuration contains four TMS molecules and no DMC molecules in the first coordination shell of Li^+, indicating that TMS has a stronger affinity to the Li^+ than EC and/or can favorably align their dipole moments in the coordination shell.

Analysis of the Li^+ coordination in the bulk electrolyte (in the middle of the simulation cell, far away from interfaces) also showed strong preference for TMS over DMC in coordination of Li^+ as illustrated in Table 2 where coordination numbers of Li^+ with atoms belonging to various electrolyte species are compared for different electrolytes. Table 2 shows that, at all TMS/DMC electrolyte compositions, the Li^+ solvation shell is dominated by TMS with only a minor contribution from DMC. In the EC/DMC(1:2.25)/$LiPF_6$ electrolyte, however, both EC and DMC solvents contribute to the Li^+ solvation almost proportionally to the bulk composition. Also, we can see that Li^+ coordination by PF_6^- anions (quantified by Li^+–P coordination numbers) significantly reduces as the concentration of TMS increases indicating increased dissolution of ion pairs in electrolytes with high TMS content. Comparison of EC- and TMS-based electrolytes with approximately the same compositions (EC/DMC(1:2.25) and TMS/DMC(1:2)) shows that the ion pairing is noticeably reduced in the TMS-based electrolyte indicating a higher dissociation of the lithium salt in the latter.

Table 2. Coordination Numbers of Li^+ in the Bulk Electrolyte

system	O (S=O, TMS or C=O, EC) within 2.8 Å	O (C=O, DMC) within 2.8 Å	P (within 5 Å)	total
TMS/DMC (1:2)	2.52	0.74	0.92	4.2
TMS/DMC (1:1)	2.86	0.54	0.85	4.2
TMS/DMC (2:1)	3.5	0.24	0.57	4.3
EC/DMC	0.65	1.94	1.1	3.7

3.2. EDL Structure. We begin our discussion of the electric double layer (EDL) structure at electrode/electrolyte interfaces (see snapshots in Figure 1c, d) by examining the composition of EDL, solvent and ion density profiles, and orientational distributions as a function of electrode potential.

3.2.1. Density Profiles. Figure 2 shows a normalized (by the bulk values) molecular center-of-mass density profiles along the z direction (perpendicular to the electrode surface) for various species comprising the TMS/DMC(1:2)/$LiPF_6$ and TMS:DMC(2:1)/$LiPF_6$ electrolytes as a function of electrode potential. Normalization by the bulk values (which correspond to densities in the middle of the simulations cell) facilitates the comparison of changes in the EDL relative to the bulk structure for different electrolyte compositions. An examination of density profiles at PZC shows that it takes about 1 nm to reach bulk densities of species, with a clearly defined interfacial layer within about 6.0 Å near the electrode surface. Integration of these densities profiles over the interfacial layer thickness (from 0 to 6.0 Å from the interface) shows that, at PZC, the densities of TMS and DMC in this layer are about a factor of 1.8–2.0 larger than in the bulk illustrating strong attractive interactions between the electrolyte and graphite that leads to some densification of the electrolyte at the uncharged graphite surface. A similar effect was observed in the electrolyte with EC/DMC solvent.[10] However, for the salt, a depletion of the Li^+ and PF_6^- anion is observed in the interfacial layer at PZC, which can be attributed to the free energy penalty associated with distortion of the Li^+ solvation shell structure necessary for a close Li^+ approach to the surface. A similar exclusion of the Li^+ from the inner solvation layer was observed for other electrolytes at neutral surfaces.[11,20] Examination of the PF_6^- anion density profiles next to the electrode shown in Figure 2h indicates that the first peaks are significantly smaller than 1.0 for TMS/DMC-based electrolytes while it is around 2.0 for EC/DMC-based electrolyte, indicating that replacement of TMS with EC allows an easier access for PF_6^- to the uncharged electrode surface.

Increasing potential from 0 to +2.4 V increases the magnitude of the first peak in TMS density profile (from about 6 to 12) and significantly narrows the peak indicating an enhanced structuring of TMS at the cathode surface. Yet, the first peak for DMC stays approximately the same. Making the electrode potential more negative from 0 to −2.7 V also increases the magnitude of the TMS first peak but significantly decreases the magnitude of the first peak for DMC indicating

dx.doi.org/10.1021/jp3054179 | J. Phys. Chem. C 2012, 116, 23871–23881

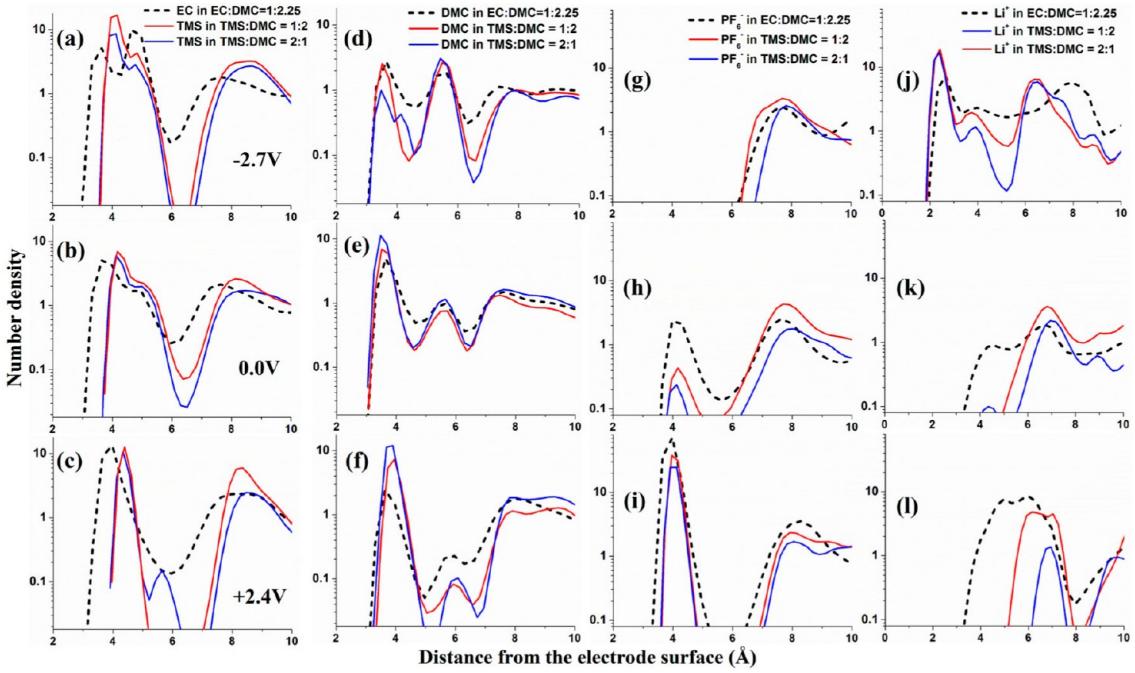

Figure 2. Normalized (by bulk values) center-of-mass number density profiles of TMS (a–c), DMC (d–f), PF_6^- (g–i), and Li^+ (j–l) for TMS/DMC = 1:2 and 2:1 at relatively high negative potential (−2.7 V, top panels), PZC (0.0 V, middle panels), and high positive potential (+2.4 V, bottom panels). Also shown for comparison are the data for electrolyte with EC/DMC = 1:2.25 solvent composition.

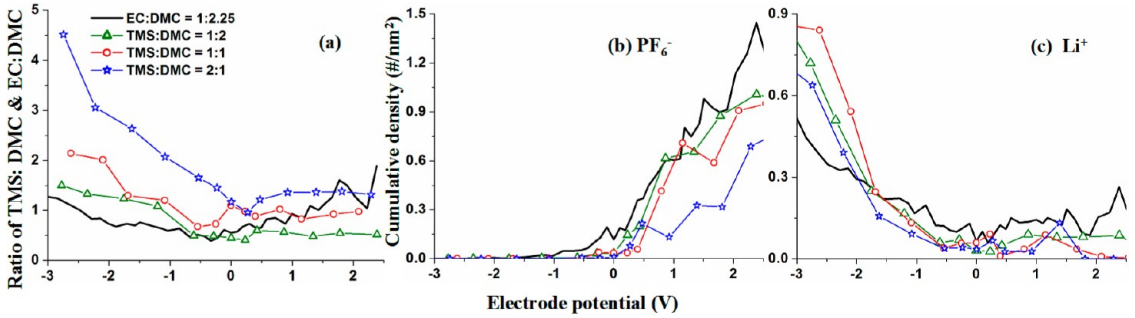

Figure 3. (a) Ratio of cumulative densities TMS/DMC and EC/DMC in the interfacial layer as a function of electrode potential. The cumulative density in the interfacial layer of PF_6^- (b) and Li^+ (c) ions as a function of electrode potential.

that, at the negative electrode, there is a significant preference for TMS presence near the surface compared to DMC. Similar trends were observed for EC and DMC in the EC/DMC(1:2.25)/$LiPF_6$ electrolyte.[10] We note that, while at PZC and positive electrode potential, DMC density profiles show two peaks within 6–7 Å from the surface with the first peak (at about 3.5–4 Å) being the dominant one, at the negative potential the DMC density profile in this region is bimodal with two equal peaks. The latter observation is indicating reorientation of DMC molecules in the interfacial layer as a function of electrode potential (see below).

Figure 2g–l shows that, during electrode charging, the counterions adsorb at electrodes forming two peaks in the center-of-mass density profile located at 2.8 Å for Li^+ and 4 Å for PF_6^- from the electrode surface. The Li^+ adsorption on the negative electrode and its strong affinity for TMS seems to explain the increased TMS adsorption and DMC desorption from the negative electrode discussed above. Comparison of density profiles for TMS/DMC(1:2)/$LiPF_6$ with results for EC/DMC(1:2.25)/$LiPF_6$ shows similar trends of electrolyte restructuring at PZC and counterion adsorption with increasing electrode potential. However, some noticeable differences in the interfacial layer structure can be also observed for the two electrolytes. For example, in the EC-based electrolyte, the Li^+ approaches the positive electrode much closer than in the TMS-based electrolyte at 0 and 2.4 V. We believe this is due to significantly higher ion pairing in the EC-based electrolyte (see discussion above of Li^+ coordination in the bulk), which results in PF_6^- adsorption together with Li^+ at the positive electrode. Also, since TMS better coordinates with Li^+ than both EC and DMC, a much more pronounced increase in the first peak of TMS compared to that of EC is observed with increasing magnitude of negative potential.

3.2.2. Interfacial Layer Composition. In order to better quantify changes in composition of the interfacial layer, we computed the cumulative density of each component in the interfacial layer as a function of applied potential by integrating density profiles from 0 to 6 Å, which corresponds to the layers shown in Figure 1c, d. The TMS/DMC ratio of densities in the interfacial layer is shown in Figure 3a as a function of applied potential. This figure illustrates the enrichment/depletion of the surface with a particular type of solvent molecules relative

dx.doi.org/10.1021/jp3054179 | J. Phys. Chem. C 2012, 116, 23871–23881

to the bulk composition. Increasing the potential on the negative electrode results in the increase of TMS concentration in the interfacial layer as the TMS is adsorbed together with Li^+ on the negative electrode due to its preferential coordination as well as large dipole model that is favored by the charged surface, while nonpolar DMC is only a minor component of the Li^+ coordination shell as seen from Table 2. On the positive electrode, however, the ratio of TMS to DMC in the interfacial layer stays approximately the same and is similar to bulk solvent ratios for TMS/DMC (1:2) and (1:1) compositions. For a TMS/DMC ratio of 2:1 composition, we observe less TMS in the interfacial layer; the TMS/DMC ratio is less than 1.5. Contrary to this result, adsorption of EC and desorption of DMC upon charging both electrodes was observed in the EC/DMC(1:2.25)/$LiPF_6$ electrolyte.[10] Hence, the polar character of the TMS molecule does not result in preferential partitioning to the positively charged surface, indicating that other factors are competing/canceling the favorable interaction of the larger TMS dipole moment with the charged surface. For example, the stronger interaction of TMS with Li^+ that is repelled by the positive electrode can represent such competing interaction. Therefore, the comparison of EC- and TMS-based electrolytes illustrates that composition of solvent molecules at electrode surfaces is a delicate balance of several competing interactions.

The cumulative densities of ions in the interfacial layer are shown in Figure 3b and c. Figure 3b shows that, in electrolytes with EC/DMC solvent, a somewhat higher accumulation of PF_6^- on the positively charged surfaces is observed compared to TMS-based electrolytes. The latter also shows a noticeable dependence of PF_6^- accumulation on the solvent composition, with electrolytes having a higher TMS content showing the smaller accumulation rate (and hence overall amount) of PF_6^- on the surface as a function of electrode potential. Figure 3c shows that Li^+ accumulation at the negative electrode is initially (from 0 to −1.8 V) faster for EC/DMC/$LiPF_6$ compared to that for TMS/DMC/$LiPF_6$ electrolytes but then becomes slower for potentials more negative than −2 V. In the potential range from 0 to −1.8 V, only few Li^+ in TMS/DMC/$LiPF_6$ electrolytes adsorb directly to the electrode surface (see Figure 2), but as potential becomes more negative than −2 V, the electrostatic attraction between Li^+ and the negative electrode becomes sufficiently large to overcome Li^+ coordination by TMS and directly adsorb onto the electrode surface. The Li^+ in TMS/DMC/$LiPF_6$ is also highly dissociated allowing it to easier adsorb on the electrode surface without the associated PF_6^- repelling the $Li_x(PF_6^-)_y$ cluster or ion pair from the negative electrode surface. Finally, Figure 3c also shows that Li^+ accumulation on the negative electrode has nonmonotonic dependence on solvent composition. While this effect is not large, nevertheless, it is clear that solvent with a 1:1 TMS/DMC ratio allows the highest amount of Li^+ adsorption to the negatively charged surface.

3.2.3. Atomic-Based Density Profiles. After examining molecular level details of the EDL, we consider EDL structure at finer level focusing on the atomistic structure of electrolyte near electrode surfaces including the orientation of solvent molecules relative to the electrode surface. Figures 4 and 5 show density profiles for the carbonyl oxygen of DMC denoted as O(═C), the DMC ether oxygen denoted as —O—, the oxygen atoms of TMS denoted as O(═S) for electrolyte with TMS/DMC(1:2) solvent composition. Also shown are density profile for carbonyl oxygen atoms of EC O(=C) for EC/DMC(1:2.25) solvent. Examination of the oxygen atom

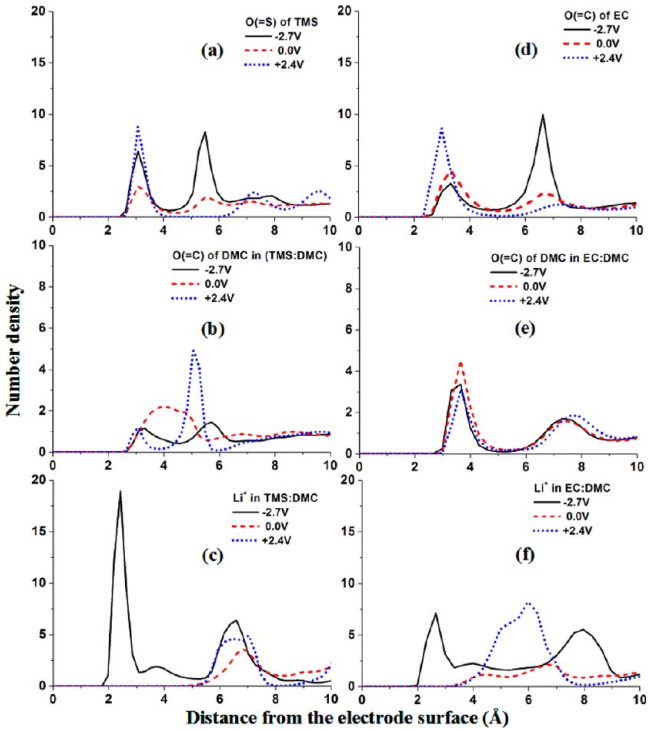

Figure 4. (a−c) Normalized atomic density profiles of O(═S) of TMS, DMC, and Li^+ in TMS/DMC 1:2; (d−f) density of O(═C) of EC, DMC, and Li^+ of EC/DMC 1:2.25 at three electrode potentials.

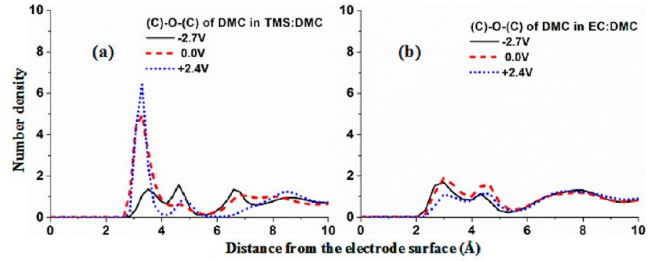

Figure 5. Normalized atomic density profiles of —O— of DMC of TMS/DMC 1:2 (a) and EC/DMC 1:2.25 (b) at three electrode potentials.

distributions near the surface shows that the magnitude of the first peak in density of TMS oxygen atoms significantly increases in magnitude as potential decreases from 0 to −2.7 V or increases from 0 to 2.4 V. The first peak for DMC O(═C) in the TMS-based electrolyte (Figure 4b) decreases in magnitude upon charging electrodes (either positive or negative) indicating that the DMC carbonyl group desorbs or reorients away from electrodes upon charging, while changes in the DMC profiles in EC/DMC/$LiPF_6$ are less pronounced. Significant changes of the DMC atomic density profiles should be contrasted with the DMC center-of-mass behavior (Figure 2), where the DMC first peak did not decrease in magnitude in the potential range from PZC to 2.4 V. This disagreement is reconciled by observation that the DMC ether oxygen (—O—) peak is well pronounced and stays almost unchanged upon charging positive electrode as can be seen from Figure 5a. The observed trends in density profiles are consistent with DMC molecule reorientation near the surface upon charging positive electrode with the carbonyl oxygen largely pointing away from the charged electrode while —O— atoms do not

dx.doi.org/10.1021/jp3054179 | J. Phys. Chem. C 2012, 116, 23871−23881

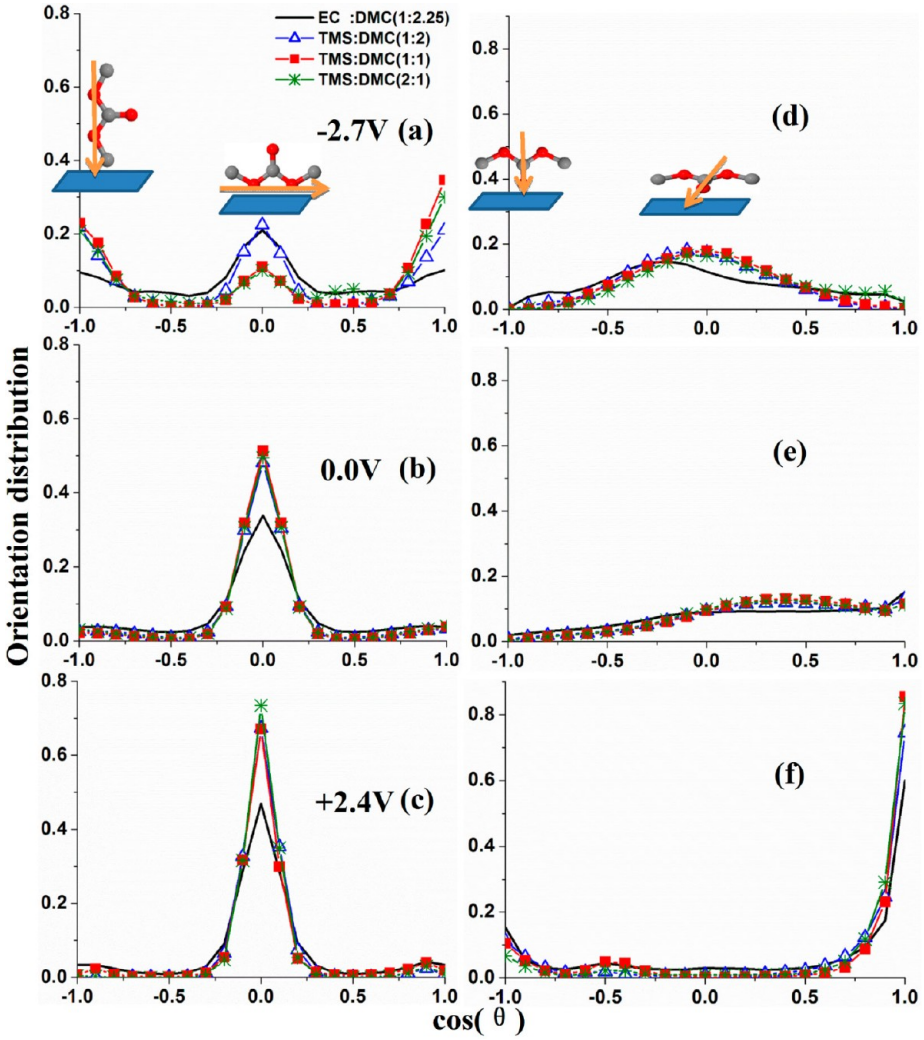

Figure 6. Orientation distributions of DMC molecules on the electrode surface in systems with TMS/DMC and EC/DMC solvents at different electrode potential: (a–c) for O_{ether}–O_{ether} vector orientation; (d–f) for C═O bond orientation. The distributions are normalized such that $\int_0^{2\pi} d\varphi \int_{-1}^{1} \rho_P d(\cos\theta) = 1$.

change their locations upon charging (Figure 5a). Thus, we conclude that —O— and O(═C) density profiles of DMC indicate a quite different orientation of DMC in EC/DMC/$LiPF_6$ and TMS/DMC/$LiPF_6$. The most significant ramification of the DMC orientational differences between EC- and TMS-based electrolytes is the observed difference in the closest approach of DMC oxygen atoms to the positive electrode surface. Specifically, DMC oxygen atoms approach as close as 2 Å in EC/DMC/$LiPF_6$, but the onset of the DMC oxygen density profiles in TMS/DMC/$LiPF_6$ is at 2.8 Å. One might expect that the further DMC atoms are away from the electrode surface the less likely it will get oxidized. Thus, DMC density profiles shown in Figures 4b, e and 5 suggest that, in TMS-based electrolytes, DMC might be more oxidatively stable than in EC-based electrolytes.

3.2.4. Solvent Orientation at Electrodes. In order to confirm our suppositions about changes in interfacial solvent orientations inferred from the atomic density profiles discussed above, we have analyzed the interfacial solvent orientation. For DMC, we considered the distribution of (i) the angle between a normal to the surface and the "elongated axis" connecting the two O(ether) atoms and (ii) the angle between the C═O bond and the normal to the electrode surface. The orientations of DMC, shown in Figure 6, are almost similar for the EC- and TMS-based systems and essentially independent of solvent concentration. However, orientation of DMC at the interface is very sensitive to the applied potential. As the potential changes from negative to positive, an increase in parallel orientation of the DMC elongated axis to the electrode surface is observed (see panels a–c). The orientation of the C═O bond, on the other hand, has a broad distribution of orientations at negative potentials, although it is centered around the orientation parallel to the surface (Figure 6d). At the PZC, the orientation distribution becomes even broader (as expected); however, the overall tendency is for the C═O groups to point away from the surface rather than toward it. At large positive potentials, DMC is primarily adsorbed on the surface with —O— atoms, and the O(═C) is pointing away from the electrode surface. Only a small percentage of DMC molecules is oriented with C═O pointing toward the surface (Figure 6f). This orientation of DMC molecules facilitates coordination with Li^+ that sits primarily outside of the interfacial layer. Figure 6c, f also indicates that DMC orientations are significantly more disordered in EC/DMC/$LiPF_6$ than in TMS/DMC/$LiPF_6$, because the magnitude of the peaks are significantly smaller in the former electrolyte, which is consistent with the significantly

dx.doi.org/10.1021/jp3054179 | J. Phys. Chem. C 2012, 116, 23871–23881

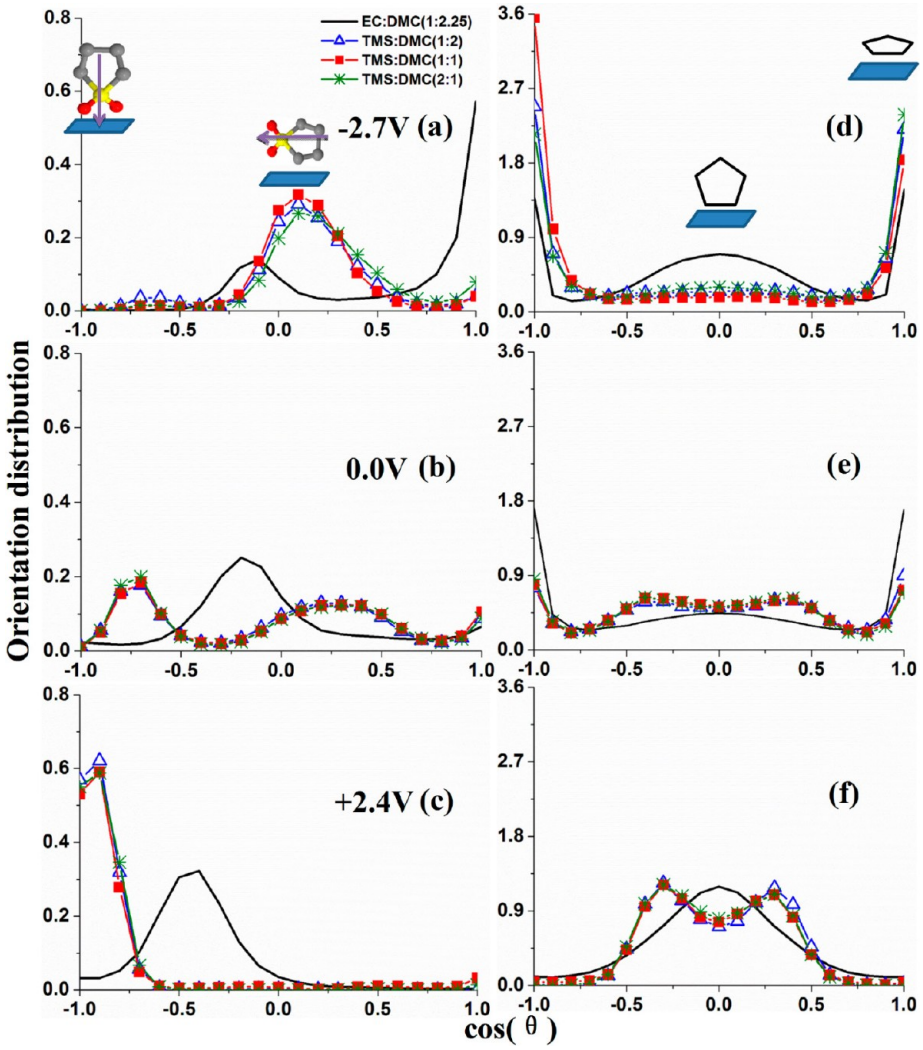

Figure 7. Orientation distributions of TMS and EC molecules in systems with TMS/DMC and EC/DMC solvents: (a−c) the angle between the ring vector shown by the arrow in panel (a) and the z axes; (e−f) the angle between the ring plane and the surface plane. The distributions from panels a−c are normalized such that $\int_0^{2\pi} d\varphi \int_{-1}^{1} \rho_P d(\cos\theta) = 1$. The distributions in panels e−f are normalized such that $\int_{-1}^{1} \rho_P d(\cos\theta) = 1$.

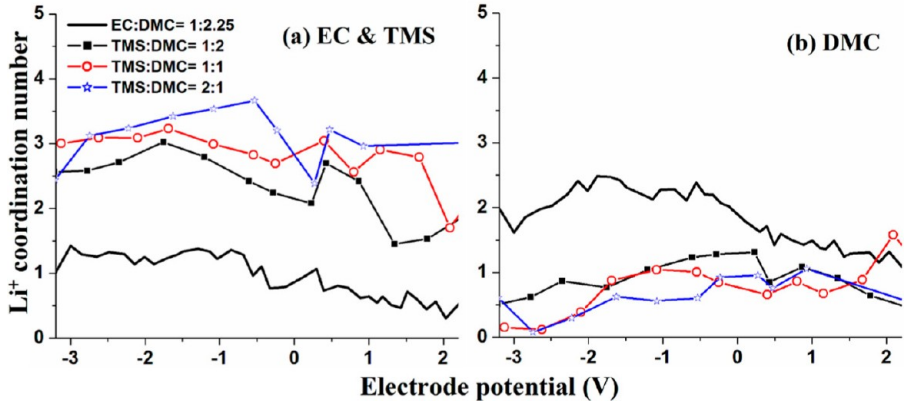

Figure 8. Coordination number of (a) EC or TMS and (b) DMC around Li^+ as a function of electrode potential.

broader density profiles shown in Figure 5 for EC/DMC/$LiPF_6$ compared to TMS/DMC/$LiPF_6$.

In order to quantify the orientation of EC and TMS molecules in the interfacial layer, two measures of orientation also were used: first, the angle between the normal to the surface and a vector connecting the middle of the ring C−C bond and S (in TMS) or the carbonyl C (in EC); second, an angle between the surface and the plane of the EC or TMS rings as illustrated on insets of Figure 7a, d. Figure 7 shows that, for TMS-based electrolytes, there is very little dependence of TMS orientation as a function of electrolyte composition. Yet, there is a significant change in TMS orientation as a function of

dx.doi.org/10.1021/jp3054179 | J. Phys. Chem. C 2012, 116, 23871−23881

potential as well as qualitatively different orientation compared to EC electrolyte. On the negative electrode surface (Figure 7a, d), the ring of the EC molecule can be parallel (with very sharp peak in the distribution) to the surface or perpendicular but with a very broad distribution, with the O(=C) atom of the carbonyl group pointing away from the surface. In contrast, for TMS, we observe a sharp distribution of parallel to the surface orientations of the ring and a smaller population of randomly oriented rings. The orientation of the "elongated axis" of EC indicates that, on the negative surface, the O(=C) predominantly points away from the surface, while TMS molecules have a tilt with the surface allowing one O to be pointed toward the surface and coordinate with Li^+. At large positive potential, EC is tilted such that one —O— and O(=C) are exposed to the surface. Similarly, perpendicular orientation of TMS on the positive surface results in both O atoms pointing toward the surface, which implies that the interfacial TMS molecules must desolvate Li^+.

3.3. Li^+ Coordination in the Interfacial Layer. Next, we examine the coordination of Li^+ located in the interfacial layer as a function of applied potential. Figure 8 shows that the total coordination number (CN) of Li^+ in the interfacial layer is essentially constant (and largely independent of solvent composition) for potentials above −2 V. Below −2 V, for the TMS-based electrolyte, Li^+ approaches the surface at a distance of about 2 Å (see density profiles in Figure 2), and therefore, its total CN with the solvent (sum of the TMS Figure 8a and DMC Figure 8b) decreases down to about 3 as the potential decreases from −2 to −3 V. Similar behavior is observed for the system with the EC/DMC solvent below −2 V.[10] At the positive electrode, the TMS and EC oxygen atoms reorient toward the electrode surface and are no longer available for Li^+ coordination, consistent with an observed slight decrease of Li^+ coordination by TMS and EC. Instead, Li^+ increasingly participates in forming ion pairs and aggregates with PF_6^- that is available in excess at the positive electrode as potential increases (see Figure 3).

Next, we examine the fraction of the interfacial solvent that participates in Li^+ coordination (see Figure 9). Solvent

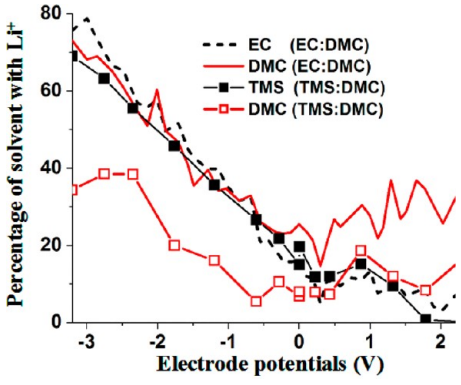

Figure 9. Percentage of interfacial solvent coordinated with Li^+ as a function of electrode potential.

molecules bound to Li^+ have higher reduction[21] and oxidation potentials due to Li^+ polarization. As electrode potential becomes more negative facilitating Li^+ adsorption, the fraction of EC and DMC that is bound to Li^+ increases and reaches 70–80% at −3 V.[10] Similar trends are also observed for the TMS–DMC/$LiPF_6$ electrolyte; however, the fraction of the interfacial DMC participating in the Li^+ complexation stays significantly lower than TMS due to significantly higher affinity of TMS to Li^+ than DMC. At the positive electrode, most of the solvent is not coordinated with Li^+ presumably due to repulsion between the positive electrode and positively charged Li^+. These results indicate that, in investigation of oxidative properties of solvent molecules, it is reasonable to focus on solvent dimers[22] or solvent–anion[23,24] complexes without Li^+ present.

3.4. Integral Electrode Capacitance. Understanding of correlations between EDL structure and capacitance is important for a number of battery electrochemical models. Also, electrolytes investigated here have been considered for application in EDL capacitors, and understanding and improving EDL capacitance are important for increasing energy density in those devices. Therefore, we also calculated the EDL integral capacitance (C_i) as $C_i = q_{electrode}/(U_{EDL} - PZC)$, which is shown in Figure 10 for TMS- and EC-based electrolytes. For

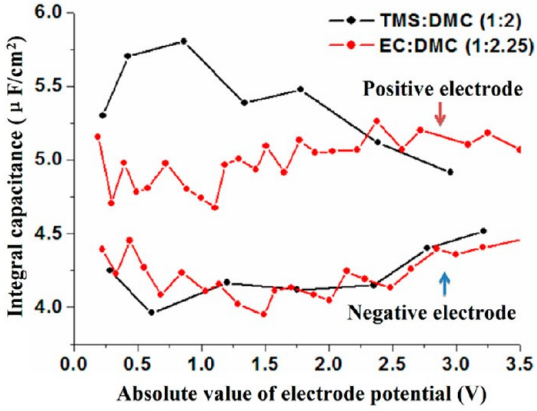

Figure 10. Electrode integral capacitance as a function of electrode potential.

both systems, C_i values are about 4–5.5 $\mu F/cm^2$, which is within the range of typically reported values from simulations of other electrode–electrolyte systems with atomically flat electrode surfaces.[10,15,16,25,26] On the negative electrode, C_i values in both systems practically stay constant over the entire range of negative potentials, and there is almost no difference between EC- and TMS-based solvents. On the positive electrode, however, below +2 V, the C_i in the TMS-based electrolyte is clearly larger (by about 0.3–0.5 $\mu F/cm^2$) than in the EC-based electrolyte. Also, the capacitance on the positive electrode is about 1–1.5 $\mu F/cm^2$ higher than the capacitance on the negative electrode. Higher capacitance on the positive electrode can be correlated with the higher rate of PF_6^- accumulation at the positive electrode compared to the rate of the Li^+ accumulation at the negative electrode upon increasing electrode potential as shown in Figure 3. In the region between −1.0 and 1.0 V, both counterion adsorption and co-ion desorption rates versus electrode potential should be taken into account when capacitance trends are explained. For example, for the potentials between −1 and 0 V, from the slower rate of Li^+ accumulation at the negative electrode in EC/DMC/$LiPF_6$ than in the TMS/DMC/$LiPF_6$ electrolyte, one can expect the higher capacitance for the latter. However, there is also significant desorption of the PF_6^- co-ion from the negative electrode in EC/DMC/$LiPF_6$ in this voltage window that boosts the capacitance value.

dx.doi.org/10.1021/jp3054179 | J. Phys. Chem. C 2012, 116, 23871–23881

4. CONCLUSIONS

The structure and composition of TMS/DMC/LiPF6 electrolytes near surfaces of graphite electrodes were investigated using MD simulations and compared with the results for the EC/DMC/$LiPF_6$ electrolyte. The interfacial layer solvent composition significantly varied as a function of potential and deviated from bulk solvent composition. Decreasing electrode potential from PZC to −2.7 V resulted in significant accumulation of TMS molecules on the negative electrode surface and desorption of DMC. This was attributed to the polar nature of TMS molecules and the Li^+ adsorption together with its first solvation shell that primarily consists of TMS molecules with only a minor contribution from DMC. On the positive electrode, TMS oxygen atoms strongly adsorbed on the surface, while DMC carbonyl groups desorbed from the positive electrode with increasing potential. The DMC oxygen atoms in TMS/DMC/$LiPF_6$ do not approach the surface of the positive electrode as close as in EC/DMC/$LiPF_6$; thus, DMC molecules in TMS/DMC/$LiPF_6$ are likely to experience lower electrochemical potential and hence are less likely to be oxidized than in EC/DMC/$LiPF_6$. This trend is consistent with experimental observations reporting that electrolytes containing a mixture of linear carbonates and TMS show high oxidative stability, similar to that observed in TMS-only electrolytes, which is higher than what is observed for electrolytes with a mixture of carbonates. Analysis of molecular level differences in EDL structure obtained from our MD simulations provides potential rationale for this trend.

Our simulations also showed that, on the negative electrode, Li^+ accumulates faster (with respect to magnitude of the electrode potential) in TMS solvent and remains strongly bound with TMS oxygen atoms even below −2 V generating surprisingly large interfacial concentration of negatively charged TMS oxygen atoms in the interfacial layer. On the positive electrode, there is a significantly smaller concentration of Li^+ in the outer part of the interfacial layer in TMS-based electrolytes than in the EC-based electrolyte, due to the fact that both oxygen atoms of the TMS molecule are adsorbed on the positively charged surface and therefore are unavailable to participate in Li^+ coordination and retain it near the surface. The $LiPF_6$ salt is completely dissociated on the negative electrode (Li^+ and PF_6^- are well separated) but are mostly associated in cation−anion pairs at the positive electrode.

AUTHOR INFORMATION

Corresponding Author

*E-mail: jenel.vatamanu@utah.edu.

Notes

The authors declare no competing financial interest.

ACKNOWLEDGMENTS

This work was supported by the Assistant Secretary for Energy Efficiency and Renewable Energy, Office of Vehicle Technologies of the U.S. Department of Energy under contract no. DE-AC02-05CH11231, subcontract no. 6838611 under the Batteries for Advanced Transportation Technologies (BATT) Program, and via an Interagency Agreement between the U.S. Department of Energy and the U.S. Army Research Laboratory under DE-IA01-11EE003413. L.X. acknowledges financial support of the Natural Science Foundation of Guangdong Province, China (grant no. 1035106310 1000001).

REFERENCES

(1) (a) Xu, K. *Chem. Rev.* **2004**, *104*, 4303−4417. (b) Zhu, K.; Wang, Q.; Kim, J.-H.; Pesaran, A. A.; Frank, A. J. *J. Phys. Chem. C* **2012**, *116*, 11895−11899. (c) Aparicio, S.; Atilhan, M. *J. Phys. Chem. C* **2012**, *116*, 12055−12065. (d) Santamaria-Perez, D.; Amador, U.; Tortajada, J.; Dominko, R.; Arroyo-de Dompablo, M. E. *Inorg. Chem.* **2012**, *51*, 5779−5786. (e) Zhang, X.; Lu., L.; Cai, Y. *Langmuir* **2012**, *28*, 9593−9600. (f) Xia, X.; Tu, J.; Zhang, Y.; Wang, X.; Gu, C.; Zhao, X-b.; Fan, H. J. *ACS Nano* **2012**, *6*, 5531−5538. (g) Lupart, S.; Gregori, G.; Maier, J.; Schnick, W. *J. Am. Chem. Soc.* **2012**, *134*, 10132−10137. (h) Rana, K.; Kucukayan-Dogu, G.; Sener Sen, H.; Boothroyd, C.; Gulseren, O.; Bengu, E. *J. Phys. Chem. C* **2012**, *116*, 11364−11369. (i) Fan, X.; Zheng, W. T.; Kuo, J.-K. *ACS Appl. Mater. Interfaces* **2012**, *4*, 2432−2438. (j) Hao, G. P.; Han, F.; Guo, D. C.; Fan, R. J.; Xiong, G.; Li, W. C.; Lu, A. H. *J. Phys. Chem. C* **2012**, *116*, 10303−10311.

(2) (a) Cresce, A. V.; Xu, K. *J. Electrochem. Soc.* **2011**, *158*, A337−A342. (b) Sathiya, M.; Hemalatha, K.; Ramesha, K.; Tarascon, J. M.; Prakash, A. S. *Chem. Mater.* **2012**, *24*, 1846−1853. (c) Wu, J.; Park, H. W.; Yu, A.; Higgins, D.; Chen, Z. *J. Phys. Chem. C* **2012**, *116*, 9427−9432. (d) Asakura, D.; Okubo, M.; Mizuno, Y.; Kudo, T.; Zhou, H.; Ikedo, K.; Mizokawa, T.; Okazawa, A.; Kojima, N. *J. Phys. Chem. C* **2012**, *116*, 8364−8369. (e) Arreaga-Salas, D. E.; Sra, A. K.; Roodenko, K.; Chabal, Y. J.; Hinkle, C. L. *J. Phys. Chem. C* **2012**, *116*, 9072−9077. (f) Valencia, H.; Kohyama, M.; Tanaka, S.; Matsumoto, H. *J. Phys. Chem. C* **2012**, *116*, 8493−8509. (g) Dathar, G. K. P.; Shelton, W. A.; Xu, Y. *J. Phys. Chem. Lett.* **2012**, *3*, 891−895. (h) Aoki, K. *Electrochim. Acta* **2012**, *67*, 216−223. (i) Du, Z.; Zhang, S. *J. Phys. Chem. C* **2011**, *115*, 23603−23609.

(3) (a) Wang, D.-W.; Zhou, G.; Li, F.; Wu, K.-H.; Lu, G. Q.; Cheng, H.-M.; Gentle, I. R. *Phys. Chem. Chem. Phys.* **2012**, *14*, 8703−8710. (b) Xing, L. D.; Wang, C. Y.; Xu, M. Q.; Li, W. S.; Cai, Z. P. *J. Power Sources* **2009**, *189*, 689−692. (c) Xing, L. D.; Li, W. S.; Xu, M. Q.; Li, T. T.; Zhou, L. *J. Power Sources* **2011**, *196*, 7044−7047. (d) Etacheri, V.; Marom, R.; Elazari, R.; Salitra, G.; Aurbach, D. *Energy Environ. Sci.* **2011**, *4*, 3243−3262. (e) Liu, J.; Zheng, Y.; Liao, Y.-P.; Zeng, X.; Ungar, G.; Wright, P. V. *Faraday Discuss.* **2005**, *128*, 363−378.

(4) Xu, K.; Angell, C. A. *J. Electrochem. Soc.* **2002**, *149*, A920−A926.

(5) Sun, X. G.; Angell, C. A. *Electrochem. Commun.* **2005**, *7*, 261−266.

(6) Abouimrane, A.; Belharouak, I.; Amine, K. *Electrochem. Commun.* **2009**, *11*, 1073−1076.

(7) Cresce, A. V.; Xu, K. *Electrochem. Solid-State Lett.* **2011**, *14*, A154−A156.

(8) Watanabe, Y.; Kinoshita, S. I.; Wada, S.; Hoshino, K.; Morimoto, H.; Tobishima, S. I. *J. Power Sources* **2008**, *179*, 770−779.

(9) Borodin, O.; Smith, G. D. *J. Phys. Chem. B* **2009**, *113*, 1763−1776.

(10) Vatamanu, J.; Borodin, O.; Smith, G. D. *J. Phys. Chem. C* **2012**, *116*, 1114−1121.

(11) Smith, G. D.; Borodin, O.; Russo, S. P.; Rees, R. J.; Hollenkamp, A. F. *Phys. Chem. Chem. Phys.* **2009**, *11*, 9884−9897.

(12) (a) Borodin, O.; Smith, G. D. *J. Phys. Chem. B* **2009**, *113*, 1763−1776. (b) Borodin, O. *J. Phys. Chem. B* **2009**, *113*, 11463−11478.

(13) Thole, B. T. *Chem. Phys.* **1981**, *59*, 341−350.

(14) Reed, S. K.; Lanning, O. J.; Madden, P. A. *J. Chem. Phys.* **2007**, *126*, 084704.

(15) Vatamanu, J.; Borodin, O.; Smith, G. D. *Phys. Chem. Chem. Phys.* **2010**, *12*, 170−182.

(16) (a) Vatamanu, J.; Borodin, O.; Bedrov, D.; Smith, G. D. *J. Phys. Chem. C* **2012**, *116*, 7940−7951. (b) Vatamanu, J.; Cao, L.; Borodin, O.; Bedrov, D.; Smith, G. D. *J. Phys. Chem. Lett.* **2011**, *2*, 2267−2272. (c) Xing, L.; Vatamanu, J.; Smith, G. D.; Bedrov, D. *J. Phys. Chem. Lett.* **2012**, *3*, 1124−1129.

(17) (a) Kawata, M.; Mikami, M. *Chem. Phys. Lett.* **2001**, *340*, 157−164. (b) Kawata, M.; Nagashima, U. *Chem. Phys. Lett.* **2001**, *340*, 165−172. (c) Kawata, M.; Mikami, M.; Nagashima, U. *J. Chem. Phys.* **2002**, *116*, 3430. (d) Kawata, M.; Mikami, M.; Nagashima, U. *J. Chem. Phys.* **2002**, *117*, 3526. (d) Kawata, M.; Mikami, M.; Nagashima, U. *J. Chem. Phys.* **2001**, *115*, 4457.

(18) Hoover, W. G. *Phys. Rev. A* **1985**, *31*, 1695−1697.
(19) Martyna, G. J.; Tuckerman, M. E.; Tobias, D. J.; Klein, M. L. *Mol. Phys.* **1996**, *87*, 1117−1157.
(20) Borodin, O.; Smith, G. D.; Bandyopadhyaya, R.; Redfern, P.; Curtiss, L. A. *Modell. Simul. Mater. Sci. Eng.* **2004**, *12*, S73−S89.
(21) Vollmer, J. M.; Curtiss, L. A.; Vissers, D. R.; Amine, K. *J. Electrochem. Soc.* **2004**, *151*, A178−A183.
(22) Xing, L.; Borodin, O. *Phys. Chem. Chem. Phys.* **2012**, *14*, 12838−12843.
(23) Borodin, O.; Jow, T. R *ECS Trans.* **2011**, *33*, 77−84.
(24) Xing, L.; Borodin, O.; Smith, G. D.; Li, W. *J. Phys. Chem. A* **2011**, *115*, 13896−13905.
(25) (a) Vatamanu, J.; Borodin, O.; Smith, G. D. *J. Am. Chem. Soc.* **2010**, *132*, 14825−14833. (b) Vatamanu, J.; Borodin, O.; Smith, G. D. *J. Phys. Chem. B* **2011**, *115*, 3073−3084.
(26) (a) Druschler, M.; Borisenko, N.; Wallauer, J.; Winter, C.; Huber, B.; Endresb, F.; Roling, B. *Phys. Chem. Chem. Phys.* **2012**, *14*, 5090−5099. (b) Rolling, B.; Druschler, M.; Huber, B. *Faraday Discuss.* **2012**, *154*, 303−311. (c) Druschler, M.; Huber, B.; Roling, B. *J. Phys. Chem. C* **2011**, *115*, 6802−6808.